# Assembling Flower-on-Sheet CoP-NiCoP Nanohybrids as Efficient Self-Supported Electrocatalysts for Hydrogen Evolution Reaction in Both Acidic and Alkaline Media

Yuqun Lin[1, =], Peican Wang[1, =], Adeline Loh[b], Lei Wan[a], Ullah Habib[b], Ziang Xu[a], Xiaohong Li[b]*, Baoguo Wang[a]*

[1] The State Key Laboratory of Chemical Engineering, Department of Chemical Engineering, Tsinghua University, Beijing 100084, P. R. China.

2 Renewable Energy Group, College of Engineering, Mathematics and Physical Sciences, University of Exeter, Penryn Campus, Cornwall TR10 9FE, UK.

*Corresponding Author.

E-mail address: bgwang@tsinghua.edu.cn (B.G. Wang); X.Li@exeter.ac.uk (X.L. Li).

=These authors contributed equally to this work

**Abstract**

Self-supported electrocatalysts are directly employed as electrodes for water splitting. Herein, we report an effective strategy to develop flower-on-sheet structured nanohybrids, where CoP nanoflowers are epitaxially grown along the edges of Ni-Co-P nanosheets (namely NiCoP) on carbon cloth (m-CoP-NiCoP/CC), thus obtained as efficient self-supported electrodes for the hydrogen evolution reaction (HER) in both acidic and alkaline media. This unique nanostructure endows NiCoP nanosheets with maximal exposed surface area, along with increased active sites brought by CoP nanoflowers. Moreover, due to good electrical connection between CoP nanoflowers and NiCoP, and between conductive NiCoP and carbon cloth, electrons can easily transfer from active sites to the conductive substrates. Therefore, the m-CoP-NiCoP/CC exhibits superior catalytic activity and stability for HER in both acidic and alkaline media. The as-prepared electrocatalyst requires overpotentials of only 75.0 and 81.5 mV to deliver a benchmark current density of 10 mA $cm^{-2}$ in acidic and alkaline media, respectively, which are superior to most of the previously reported metal phosphides based electrocatalysts. Hence, this work can provide a design for developing highly active electrocatalysts for water splitting.

*Keywords:* electrocatalysts, CoP-NiCoP nanohybrids, flower-on-sheet structure, acidic and alkaline media, hydrogen evolution reaction.

## 1. Introduction

Hydrogen generation via water splitting is a promising way to realize economic hydrogen. Over the last two decades, many water dissociation devices are proposed, which are mainly based on proton exchange membranes (PEM) and work in strongly acidic media [1,2]. However, PEM water electrolysis method produces expensive hydrogen due to heavy dependence on expensive membranes and precious metal catalysts. To date, alkaline water electrolysis is known as the only matured and commercialized electrolysis among all kinds of water electrolysis. Transition metals, such as sulfides [3-5], selenides [6], and phosphides [7-9], have been extensively explored as electrocatalysts for HER due to their low cost. However, their catalytic performance is still far from satisfactory. Furthermore, it is desirable to develop high-performance electrocatalysts that can operate in a wide pH range, which can significantly reduce the energy efficiency loss during long-term electrolysis, satisfy the complicated application criteria and reduce the processing complexity. Therefore, developing efficient, low-cost, and durable HER electrocatalysts in both acidic and alkaline solution is urgently needed.

Among all transition metal materials, the transition-metal phosphides such as cobalt phosphides, have shown promising catalytic activity toward HER in both acidic and alkaline environments [10-12]. For instance, Wu et al. constructed nitrogen-doped nanoporous graphitic carbon membranes functionalized with Janus-type Co/CoP nanocrystals, which show overpotentials of 125 and 138 mV at a current density of 10 mA $cm^{-2}$ in acidic and alkaline conditions, respectively [11]. Despite progress made,

the catalytic performance and stability are still far from satisfactory. Therefore, the development of highly active cobalt-phosphide-based electrocatalysts remains a challenging task.

To enhance the catalytic activity of catalysts, many studies are focusing on tailoring the exposed active sites by optimizing the morphology and surface areas of the materials [12,13]. Hence, various structures have been intensively investigated including nanosheets [14-16], nanotubes [17], nanowires [18], hollow and branched nanostructures [19,20]. These structures result in the highly exposed active site, fast transportation of electrolyte, and gas bubble release, which consequently enhance the catalytic activity.

Moreover, the combination of different active materials is also reported for improved catalytic activity [15,21-24]. However, the active sites of primary material are usually covered by the secondary component which somehow deteriorates the activity of primary material. Furthermore, to our knowledge, none of works focused on combining two kinds of structures with minimal contacts whose performance improvement mainly comes from increased active sites rather than synergistic effect, such as nanoflowers epitaxially grown along the edges of nanosheet (flower-on-sheet), increasing surface areas brought about by secondary component and highly exposed active sites of the primary component.

Self-supported electrocatalysts have been directly employed as electrodes which are intensively studied for water splitting and found to have favorable catalytic performance. An integrated electrode is easier to achieve favorable surface properties

by purposefully tailoring the surface structure and morphology [25-27]. Hence, the fabrication of a self-supported electrode can be an effective approach to developing high-performance electrocatalysts.

In this work, we develop an efficient and robust electrode for HER from flower-on-sheet structured nanohybrids of cobalt and Ni-doped cobalt phosphides on carbon cloth, for HER in both acidic and alkaline media. Co-based metal-organic framework (Co-MOF) derived CoP nanoflowers (m-CoP) are designed and epitaxially grown along the edges of Ni-Co-P nanosheets (namely NiCoP) arrays on carbon cloth (m-CoP-NiCoP/CC). Benefiting from the design of this unique structure, the CoP nanoflowers on the lateral edges of nanosheets provide an effective exposure of the NiCoP nanosheets layer, which can enlarge the surface exposure areas of NiCoP nanosheets and perfectly maintain gas diffusion channels. This structure increases active sites by CoP nanoflowers and enhances the HER electrocatalytic activity.

## Experimental

### *2.1 Synthesis of Ni-doped $Co(OH)_2$ nanosheets on carbon cloth (Ni-Co-OH/CC)*

The Ni-Co-OH/CC was prepared by one-step electrodeposition in a three-electrode cell (**Fig. S1**). The saturated calomel electrode (SCE) and a 2×2 cm Pt foil were used as reference and counter electrodes, respectively. A 1×1 cm carbon cloth was first cleaned in 3M HCl, ethanol, and deionized water and used as a working electrode. The electrodeposition was carried out under the fixed potential (vs. SCE) of -1 V with different deposition timespan in a range from 200 to 800 sec, in an electrolyte consisting of 0.2 M $Co(NO_3)_2$ and 0.1 M $Ni(NO_3)_2$ and a 100 mL beaker without stirring. The

prepared sample (Ni-Co-OH/CC) was washed with water and dried in air for several hours.

*2.2 Synthesis of Ni-Co-OH supported Co-MOF on carbon cloth (Co-MOF-Ni-Co-OH/CC)*

Preparation of Co-MOF-Ni-Co-OH/CC is similar to that of Ni-Co-OH/CC, where the deposition is performed at a fixed potential (vs. SCE) of -5 V in the electrolyte consisting of 0.1 M $Co(NO_3)_2$ and 0.8 M 2-methylimidazole in 95% methanol solution with different deposition time, using Ni-Co-OH/CC as working electrode. The prepared sample was dried in air overnight [28].

*2.3 Synthesis of the m-CoP-NiCoP/CC*

The as-prepared Co-MOF-Ni-Co-OH/CC and 1.0 g $NaH_2PO_2$ were put into a crucible and annealed at 400 °C for 120 min, under an Ar atmosphere (100 sccm) with a heating speed of 2 °C $min^{-1}$. Then, the prepared samples were immersed in deionized water for several hours and then took out and washed with deionized water and alcohol, several times. For comparison, the Ni-Co-OH/CC and bare Co-MOF/CC were also converted into NiCoP/CC and m-CoP/CC by phosphorization treatment.

*2.4 Characterizations*

The structure of all samples was first characterized by scanning electron microscope (SEM, Merlin, Carl Zeiss) at 5 kV. The detailed structure of m-CoP-NiCoP was further confirmed using transmission electron microscopy (TEM) and high-resolution TEM (HR-TEM) on a JEOL JEM-2010 (Japan) microscope at 120 kV and the corresponding energy-dispersion X-ray spectroscopy (EDS) was used to analyze

elementary distribution. The crystal structures of all sample were identified by x-ray diffraction (XRD, Bruker D8 Advance) with Cu Kα (λ = 0.15406 nm) radiation. The X-ray photoelectron spectroscopy (XPS) was performed on an ESCALAB 250Xi with Al Kα X-ray radiation. All XPS data were corrected by C 1s line. The software used for XPS data analysis is XPSPEAK41.

*2.5 Electrochemical measurements*

All the electrochemical characterizations were carried out in a traditional three-electrode cell, using an electrochemical workstation (VersaSTAT-3F) at room temperature. The as-prepared sample with a geometric area of 1 $cm^2$ was directly used as a working electrode, and the Pt foil was used as a counter electrode. For the HER measurement in acidic solution (0.5 M $H_2SO_4$), the saturated calomel electrode (SCE) was used as the reference electrode. The polarization curves were tested at a potential sweep rate of 5 mV $s^{-1}$. The Tafel slope was fitted by polarization curves in the strongly polarized region. All of the above data was corrected by iR compensation. All potentials were also converted to the reversible hydrogen electrode (RHE) with the help of equation 1: $E = E_{SCE} + 0.241 + 0.059(1)$.

For the HER measurement in 1 M KOH solution, all tested were carried out in a similar way to that of acidic solution, except the SCE was replaced by the Hg/HgO electrode and the potentials were converted by the following equation: $E = E_{HgO/Hg} + 0.098 + 0.059\,pH$. The electrochemical impedance spectroscopy (EIS) was measured at AC impedance with an amplitude of 10 mV and a frequency range of 100 to 0.01 Hz. The electrochemical surface area (ECSA) was calculated by double-layer

capacitances based on the cyclic voltammograms (CVs) at different scan rates.

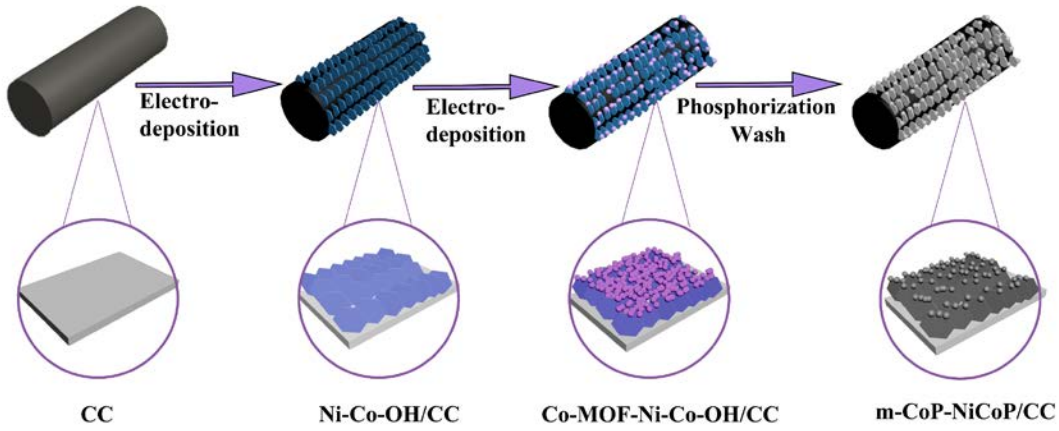


**Fig. 1.** Schematic illustration of fabrication of flower-on-sheet m-CoP-NiCoP/CC nanohybrids.

## 3. Results and discussions

### *3.1 Characterizations of flower-on-sheet m-CoP-NiCoP/CC*

The synthesis of m-CoP-NiCoP/CC electrodes involves a three-step process, as depicted in **Fig. 1**. First, the Ni-doped $Co(OH)_2$ nanosheets (Ni-Co-OH/CC) arrays were vertically grown on the surface of carbon cloth. Second, the Ni-Co-OH was used as an electrode for the electrodeposition of Co-MOF (m-Co-MOF-Ni-Co-OH/CC). The color of electrode becomes pink after the electrodeposition of Co-MOF. Finally, the m-Co-MOF-Ni-Co-OH/CC was converted into m-CoP-NiCoP/CC by the phosphorization treatment.

The SEM images of m-CoP-NiCoP/CC at different magnifications are shown in **Fig. 2a-c**. It shows that the Co-MOF derived CoP is epitaxially grown along the lateral edges of the NiCoP nanosheets. This unique structure prevents the NiCoP nanosheets from being covered, which can enlarge the exposure of the surface areas of NiCoP

nanosheets and increase active sites brought about by the introduction of CoP. To gain further insight into the structure of m-CoP-NiCoP/CC, the TEM and HR-TEM analysis are performed. The CoP exhibits a nanoflower-like structure (**Fig. 2d**), with a particle size of around 80 nm. The HR-TEM image (**Fig. 2e**) demonstrates that the CoP exhibits a lattice fringe spacing of the 0.277 nm, corresponding to the (011) planes of the CoP. Moreover, the EDS elemental mapping suggests the uniform distribution of Co and P (**Fig. S2**), in which the atomic ratio of Co/P is closed to 1:1. The NiCoP nanosheets were also tested by TEM and HR-TEM (**Fig. 2f and the inset**). The lattice fringes with interplanar spacings of 0.282 and 0.251 nm in HR-TEM images of the nanosheets correspond to the (011) and (111) planes of the Ni-doped CoP nanosheets (**Fig. 2f**). The slight decrease in the interplanar distance of (011) plane in NiCoP confirms the successful substitution of Ni into CoP. The EDX elemental mapping further confirms the homogenous dispersion of Co, Ni and P throughout the NiCoP nanosheets (**Fig. S3**), in which the atomic ratio of Co/Ni/P is closed to 2:1:3.

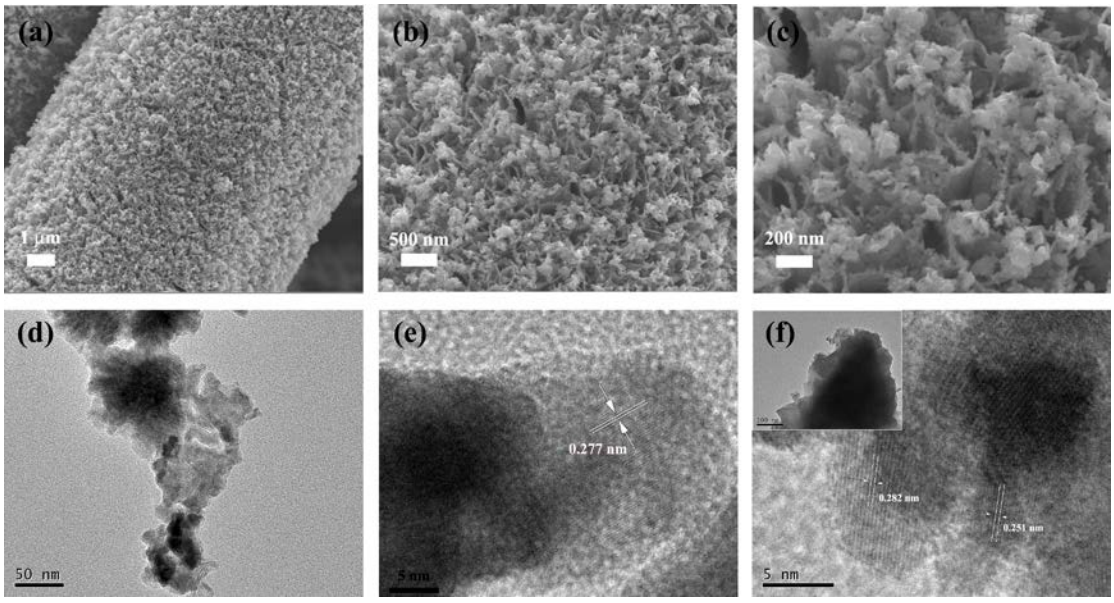


**Fig. 2.** The morphology structure of the m-CoP-NiCoP/CC. (a-c) SEM images with

different magnification of the m-CoP-NiCoP/CC. (d) The TEM image of the CoP nanoparticles. (e) HR-TEM image of the CoP nanoparticles. (f) HR-TEM image of the NiCoP, the inset is the TEM image of NiCoP nanosheets.

X-ray diffraction (XRD) was employed to further identify the components and crystallinity of the samples. **Fig. 3a** shows the XRD pattern of m-CoP-NiCoP/CC, m-CoP/CC, and NiCoP/CC. The peaks at around 25.5° and 43.5°, marked by *, which are attributed to the carbon cloth substrate [3]. It is noted that the m-CoP-NiCoP/CC, m-CoP/CC, and NiCoP/CC have similar XRD patterns. In the case of m-CoP/CC, the distinct diffraction peaks located at the 31.6°, 36.5°, 46.3°, 48.4°, 52.4° and 56.6° correspond to the (011), (111), (112), (202), (103) and (301) planes of the CoP (PDF#29-0497), respectively. The XRD patterns also show that the peaks of NiCoP and m-CoP-NiCoP are slightly shifted to the low-angle direction compared to that of m-CoP, suggesting the successful substitution of Ni into CoP. It is noteworthy that m-CoP-NiCoP/CC exhibits a similar XRD pattern compared to that of the bare NiCoP/CC, which may be attributed to the relatively low crystallization of the bare CoP nanoflowers on the lateral edges of NiCoP nanosheets. The XRD pattern of m-CoP-NiCoP/CC exhibits a typical orthorhombic CoP XRD pattern [29]. These results confirm the synthesis of flower-on-sheet m-CoP-NiCoP nanohybrids on carbon cloth.

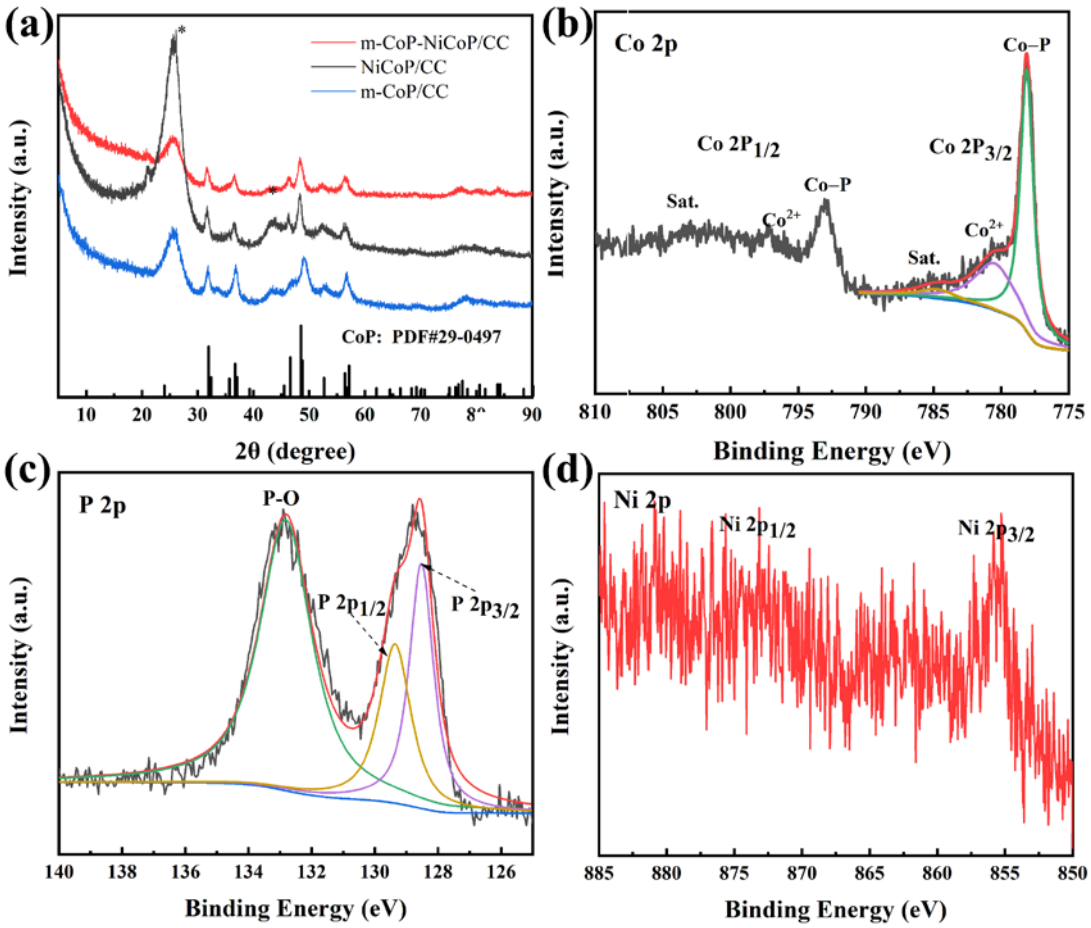


**Fig. 3.** Characterization of m-CoP-NiCoP/CC electrode. (a) XRD patterns of m-CoP-NiCoP/CC, m-CoP /CC, and NiCoP/CC. XPS spectra of m-CoP-NiCoP/CC: (b) Co 2p; (c) P 2p; (d) Ni 2p.

X-ray photoelectron spectroscopy (XPS) was conducted to probe the chemical and electronic states of m-CoP-NiCoP. The result confirms that the atomic molar ratio of Co/Ni is close to 2:1. The spectrum of Co 2p3/2 (Fig. 3b) is deconvolved into three subpeaks at 778.1, 780.5 eV and 784.7 eV, which corresponds to the Co-P bonds, oxidized cobalt ($Co^{2+}$), and satellite peak [14,15,30-33]. The presence of oxidized cobalt species is attributed to the oxidation of surface due to air exposure. The high-resolution P 2p spectrum (**Fig. 3c**) is also deconvoluted into peaks at 128.5 and 129.4 eV, corresponding to $P_{3/2}$ and $P_{1/2}$, along with a peak at 132.8 eV attributable to oxidized

phosphorus [13]. The oxidization of phosphide arises from superficial oxidation of CoP because of air contact [34]. It is noted that the negative shift of $P_{3/2}$ compared to bare elemental P is due to the incorporation of Ni. The high-resolution Ni 2P spectrum (**Fig. 3d**) reveals the peak at a binding energy of 855.28 eV corresponding to the Ni $2p_{3/2}$, which mainly originates from oxidized nickel species [35]. The noise of the Ni 2p data is because of the presence of CoP. Again, these results validate the fabrication of m-CoP-NiCoP.

*3.2 Catalytic activity of HER catalyst*

The electrochemical HER activity of the m-CoP-NiCoP was first measured in 0.5 M $H_2SO_4$. The bare m-CoP and NiCoP were also prepared for comparison (**Fig. S4**). **Fig. 4a** shows the polarization curves of m-CoP-NiCoP with different electrodeposition times of the Ni-Co-OH and with a fixed electrodeposition time of Co-MOF. The performance of m-CoP-NiCoP increases along with the increase in electrodeposition time and reaches to the maximum at 400 s. Hence, a Ni-Co-OH electrodeposition time of 400 s is adopted for further investigation. **Fig. S5** displays the influence of electrodeposition time on Co-MOF, which exhibits the best HER performance around 300 to 400 s. As shown in Fig. **S6**, the number of the Co-MOF on Ni-Co-OH nanosheets with the electrodeposition time (300 s and 400 s) is larger than the samples with the electrodeposition time of 100 s and 200 s, which will increase surface area. A Co-MOF electrodeposition time of 350 s is thereby used for further study. Moreover, the comparison of the samples with different electrodeposition time of Ni-Co-OH and Co-MOF is listed as **Table S1**. As shown in **Fig. 4b**, as expected, m-CoP-NiCoP electrodes

exhibit the best HER catalytic activity among three samples. The design of m-CoP-NiCoP significantly enhances the HER performance with an overpotential at a current density of 10 mA $cm^{-2}$, reduced from 120 mV for m-CoP and 107 mV for NiCoP, to 75 mV for m-CoP-NiCoP.

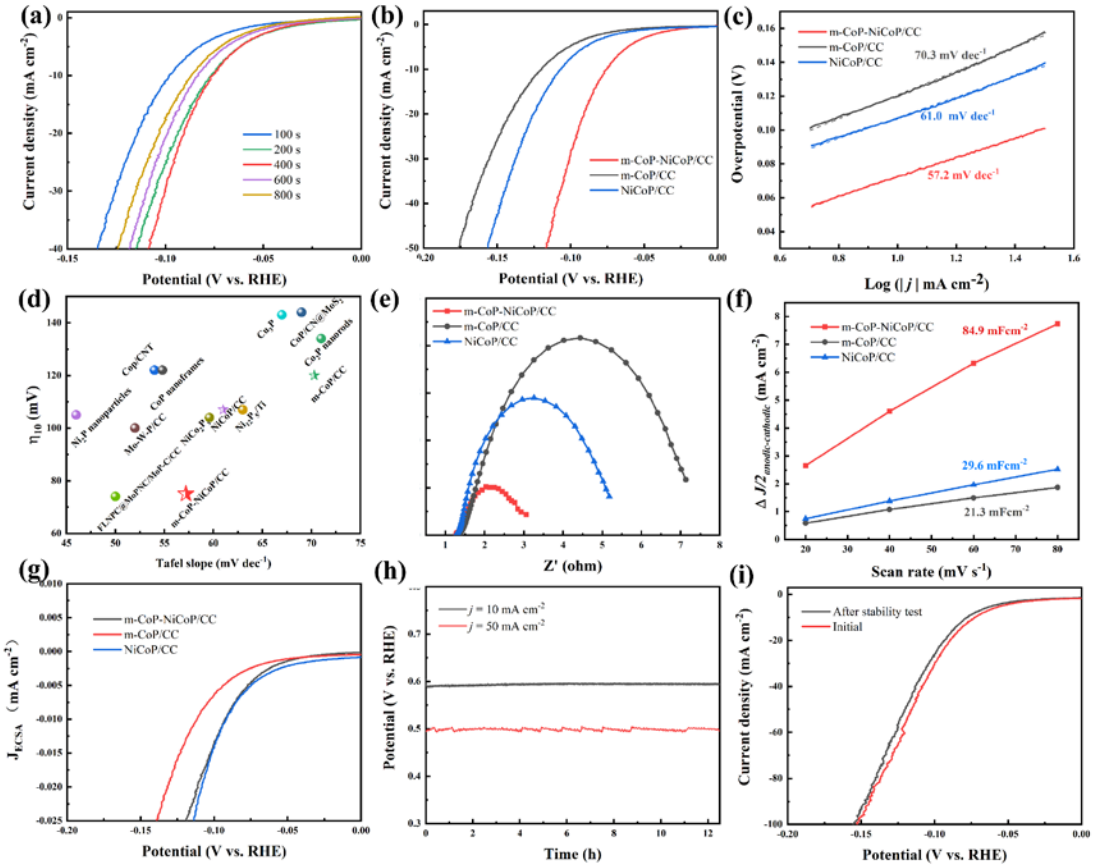


**Fig. 4.** Electrochemical measurements of different electrodes during HER in acidic solution (0.5 M $H_2SO_4$). (a) Polarization curves of m-CoP-NiCoP/CC at different electrodeposition times of Ni-Co-OH. (b) Polarization curves of m-CoP-NiCoP/CC, m-CoP /CC, and NiCoP/CC. (c) Corresponding Tafel plots. (d) Comparison of catalytic activities towards the HER with literature. (e) EIS Nyquist plots of the m-CoP-NiCoP/CC, m-CoP /CC, and NiCoP/CC electrodes. (f) Double-layer capacitances of the m-CoP-NiCoP/CC, m-CoP /CC, and NiCoP/CC electrodes. (g) Polarization curves of m-CoP-NiCoP/CC and NiCoP/CC based on ECSA. (h) Long-term stability test

carried out at constant current densities of 10 and 50 mA $cm^{-2}$. (i) Polarization curves of m-CoP-NiCoP/CC electrode before and after the chronopotentiometric measurement.

In addition, the HER kinetics were further investigated by Tafel slope. In acidic electrolyte, the first step of HER process is hydrogen adsorption, involving Volmer reaction ($H_3O^+ + e \rightarrow H^* + H_2O$, whereas H* represents the adsorbed H atom), followed by Heyrovsky reaction ($H^* + H_3O^+ + e \rightarrow H_2 + H_2O$) or Tafel reaction ($H^* + H^* \rightarrow H_2$) [36]. The theoretical Tafel slope is 120, 40 and 30 mV $dec^{-1}$ for Volmer, Heyrovsky, and Tafel reaction, respectively [37]. As shown in **Fig. 4c**, the Tafel value of m-CoP-NiCoP is 57.2 mV $dec^{-1}$, which is much smaller than that of m-CoP and NiCoP, indicating a faster HER process. The Tafel slope of m-CoP-NiCoP also suggests that the HER process is through a Volmer-Heyrovsky mechanism. The HER performance of m-CoP-NiCoP is also comparable to most of the previous reports (**Fig. 4d**), including Mo-W-P/CC (100 mV, 52 mV $dec^{-1}$) [38], CoP nanoframes (122 mV, 54.8 mV $dec^{-1}$) [10], CoP/CNT (122 mV, 54 mV $dec^{-1}$) [39], $NiCo_2P_x$ (104 mV, 59.6 mV $dec^{-1}$) [40], $Ni_2P$ nanoparticles (105 mV, 46 mV $dec^{-1}$) [41], etc. [9,18,42-44]. These results demonstrate the exceptional catalytic performance of the as-prepared catalysts.

The electrode kinetics was further investigated by electrochemical impedance spectroscopy (EIS), corresponding Nyquist plots were fitted by a simple equivalent circuit (**Fig. S7**). As shown in **Fig. 4e**, all test samples exhibit a similar solution resistance ($R_s$) of ~1.3 Ω, indicating good contact between electrode and electrolyte. Moreover, the m-CoP-NiCoP also possesses lower charge-transfer resistance ($R_{ct}$) of 1.6 Ω than m-CoP (5.57Ω) and NiCoP (3.81Ω), suggesting fast charge transfer between

CoP nanoflowers and NiCoP nanosheets due to the high conductivity of NiCoP nanosheets. In addition, the electrochemical surface area (ECSA) was estimated to obtain further insight into HER activity, which was evaluated by the double-layer capacitances ($C_{dl}$) due to their positive correlation [45]. The $C_{dl}$ values can be calculated through CVs in the non-Faradic region (**Fig. S8)**. Compared to NiCoP (29.6 mF $cm^{-2}$) and m-CoP (21.3 mF $cm^{-2}$), the m-CoP-NiCoP shows a large $C_{dl}$ value of 84.9 mF $cm^{-1}$, which is about three times as high as that of NiCoP and m-CoP (**Fig. 4f)**. Therefore, the m-CoP-NiCoP exhibits a large surface area, which is beneficial for HER activity.

To unveil the exact origin of enhanced catalytic activity, the current density is normalized by ECSA (**Fig. 4g**) [37,35]. The activity of m-CoP-NiCoP is closer to NiCoP and larger than m-CoP. Hence, the enhancement of HER performance is mainly attributed to the increase of the surface area and active sites brought about by the CoP nanoflowers rather than the synergistic effect between CoP and NiCoP. The m-CoP-NiCoP electrode exhibits favorable kinetics toward HER, which can be attributed to the following reasons: (1) the strong contact of CoP nanoflowers and high-conductivity NiCoP nanosheets, which gives rise to an excellent electrical and mechanical connection, facilitating electron transport. (2) the design of the flower-on-sheet structure with CoP nanoflowers epitaxially grown along the edges of NiCoP nanosheets, maximizing the surface exposure areas of NiCoP nanosheets and increasing active sites through CoP nanoflowers. (3) The flower-on-sheet structure well maintains the diffusion channels of NiCoP nanosheet arrays for the penetration of electrolyte and release the gaseous bubbles.

Stability is another important factor to evaluate the catalytic performance of the catalysts. As shown in **Fig. 4h,** the chronopotentiometry tests without iR correction were carried out at current densities of 10 and 50 mA $cm^{-1}$. No dramatic change in the potential is observed after the stability test, confirming the excellent stability of m-CoP-NiCoP. The fluctuation can be detected in **Fig. 4h** at a current density of 50 mA $cm^{-2}$, which is caused by the release of gas bubbles under large current density. The polarization curves before and after the chronopotentiometry test were also performed (**Fig. 4i**). There is only a slight decrease in the current density. The surface morphology and chemical composition of m-CoP-NiCoP after stability tests were further confirmed by SEM and XRD. As shown in **Fig. S9 and S10**, no obvious changes are found on the surface structure and crystal structure, after the HER process. These results confirm the excellent stability of m-CoP-NiCoP/CC electrode.

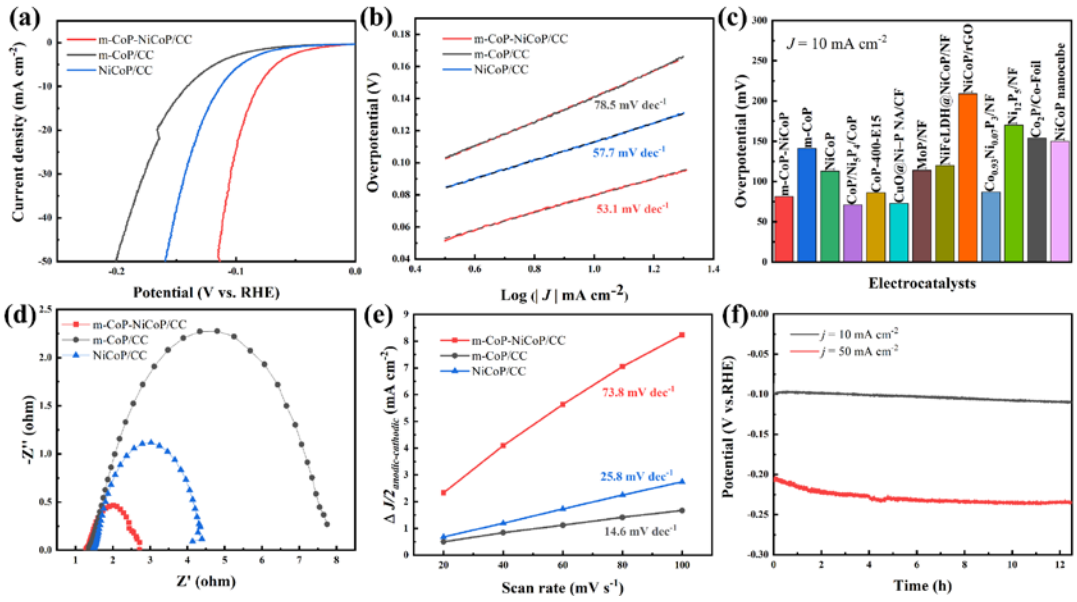


**Fig. 5.** Electrochemical measurements of different electrodes during HER in alkaline solution (1 M KOH). (a) Polarization curves of m-CoP-NiCoP/CC, m-CoP /CC, and

NiCoP/CC. (b) Corresponding Tafel plots. (c) Comparison of catalytic activities towards the HER with literature. (d) EIS Nyquist plots of the m-CoP-NiCoP/CC, m-CoP /CC, and NiCoP/CC electrodes. (e) $C_{dl}$ of the m-CoP-NiCoP/CC, m-CoP /CC, and NiCoP/CC electrodes. (f) Long-term stability test carried out at constant current densities of 10 and 50 mA $cm^{-2}$.

The m-CoP-NiCoP electrocatalyst also shows favorable HER performance in alkaline solution (1M KOH). **Fig. S11 and S12** demonstrate that m-CoP-NiCoP exhibits the best HER activity with the electrodeposition time for Ni-Co-OH of 400 s and Co-MOF of around 350 s. Moreover, the comparison of the samples with different electrodeposition time of Ni-Co-OH and Co-MOF is listed as **Table S1.** In addition, as shown in the **Fig. 5a and 5b,** the m-CoP-NiCoP required only 81 mV of overpotential to deliver 10 mA $cm^{-2}$, along with a Tafel slope of 53.1 mV $dec^{-1}$, which is much smaller than that of m-CoP (141 mV, 78.5 mV $dec^{-1}$) and that of NiCoP (112 mV, 57.7 mV $dec^{-1}$). The catalytic activity is also comparable to the recently reported effective metal phosphides (**Fig. 5c**), including CoP/$Ni_5P_4$/CoP (71 mV) [46], CoP-400-E15 (86 mV) [47], CuO@Ni-PNA/CF (73 mV) [48], MoP/NF (114 mV) [49], $Co_{0.93}Ni_{0.07}P_3$/NF (87 mV) [50], etc. [51-55]. The EIS further confirms the fast charge transfer between CoP nanoflowers and NiCoP nanosheets (**Fig. 5d**). Furthermore, the $C_{dl}$ was obtained from CV (**Fig. S13**). The m-CoP-NiCoP possesses a larger $C_{dl}$ value of 73.8 mF $cm^{-2}$ than m-CoP (14.6 mF $cm^{-2}$) and NiCoP (25.8 mF $cm^{-2}$), implying a larger ECSA (**Fig. 5e**). Besides, the chronopotentiometry measurements without iR correction (**Fig. 5f**) at fixed current densities of 10 and 50 mA $cm^{-2}$ were performed. The potential decreased slightly

and then plateaued after the decay. A comparative analysis of these results demonstrates the highly active catalysts of m-CoP-NiCoP with high stability in alkaline solution. The table below shows the main electrochemical parameters of three types of electrode.

**Table 1.** The main HER electrochemical parameters of all electrodes.

| Sample | Test environment | Overpotential at 10 mA $cm^{-2}$ | Tafel Slope (mV $dec^{-1}$) |
|---|---|---|---|
| m-CoP-NiCoP/CC | 0.5 M $H_2SO_4$ | 75 | 57.2 |
| m-CoP/CC | 0.5 M $H_2SO_4$ | 120 | 61.0 |
| NiCoP/CC | 0.5 M $H_2SO_4$ | 107 | 70.3 |
| m-CoP-NiCoP/CC | 1 M KOH | 81 | 53.1 |
| m-CoP/CC | 1 M KOH | 141 | 78.5 |
| NiCoP/CC | 1 M KOH | 113 | 57.7 |

## 4. Conclusion

In this work, a facile strategy has been developed to fabricate self-supported m-CoP-NiCoP nanohybrids on carbon cloth for hydrogen evolution reaction in both acidic and alkaline media. It shows that the CoP nanoflowers play a key role in HER activity, while NiCoP nanosheets can provide effective mass transfer channels and serve as electron transport substrate for CoP nanoflowers with the maximum surface exposure areas and active sites of NiCoP. Benefiting from these features, the m-CoP-NiCoP/CC electrode exhibits high activity with low overpotentials and small Tafel slopes (**Table 1**) for HER in acidic and alkaline media, respectively. This work can provide a design for the development of highly active electrocatalysts for HER or OER, as well as overall water splitting.

### Declaration of interests

The authors declare that they have no known competing financial interests or personal relationships that could have appeared to influence the work reported in this paper.

## Acknowledgments

This work was supported by the National Key R&D Program of China (2018YFE0202001) and the Nation Natural Science Foundation of China (21776154).

## Reference

[1] Marshall A, Børresen B, Hagen G, Tsypkin M, Tunold R (2007) Hydrogen production by advanced proton exchange membrane (PEM) water electrolysers—Reduced energy consumption by improved electrocatalysis. Energy 32 (4):431-436. https://doi.org/10.1016/j.energy.2006.07.014

[2] Lei Q, Wang B, Wang P, Liu S (2019) Hydrogen generation with acid/alkaline amphoteric water electrolysis. J Energy Chem 38:162-169. https://doi.org/10.1016/j.jechem.2018.12.022

[3] Wang P, Wan L, Lin Y, Wang B (2019) $MoS_2$ supported $CoS_2$ on carbon cloth as a high-performance electrode for hydrogen evolution reaction. Int J Hydrogen Energy 44 (31):16566-16574. https://doi.org/10.1016/j.ijhydene.2019.04.195

[4] Wang H, Li Y, Li Y, He B, Wang R, Gong Y (2018) MOFs-derived hybrid nanosheet arrays of nitrogen-rich $CoS_2$ and nitrogen-doped carbon for efficient hydrogen evolution in both alkaline and acidic media. Int J Hydrogen Energy 43 (52):23319-23326. https://doi.org/10.1016/j.ijhydene.2018.10.178

[5] Shao M, Wang P, Wang Y, Wang B, Wang Y, Xu J (2020) Continuous Synthesis of Few-layer $MoS_2$ with highly Electrocatalytic Hydrogen Evolution. Green Energy Environ. https://doi.org/10.1016/j.gee.2020.04.008

[6] Wei L, Luo J, Jiang L, Qiu L, Zhang J, Zhang D, Xu P, Yuan D (2018) $CoSe_2$ nanoparticles grown on carbon nanofibers derived from bacterial cellulose as an efficient electrocatalyst for hydrogen evolution reaction. Int J Hydrogen Energy 43 (45):20704-20711. https://doi.org/10.1016/j.ijhydene.2018.09.151

[7] Yan X, Wang G, Zhang Y, Guo Q, Jin Z (2020) 3D layered nano-flower $MoS_x$ anchored with CoP nanoparticles form double proton adsorption site for enhanced photocatalytic hydrogen evolution under visible light driven. Int J Hydrogen Energy 45 (4):2578-2592. https://doi.org/10.1016/j.ijhydene.2019.11.227

[8] Chen Z, Jia H, Yuan J, Liu X, Fang C, Fan Y, Cao C, Chen Z (2019) N, P-co-doped carbon coupled with CoP as superior electrocatalysts for hydrogen evolution reaction and overall water splitting. Int J

Hydrogen Energy 44 (45):24342-24352. https://doi.org/10.1016/j.ijhydene.2019.07.185

[9] Xie J-Y, Liu Z-Z, Li J, Feng L, Yang M, Ma Y, Liu D-P, Wang L, Chai Y-M, Dong B (2020) Fe-doped CoP core–shell structure with open cages as efficient electrocatalyst for oxygen evolution. J Energy Chem 48:328-333. https://doi.org/10.1016/j.jechem.2020.02.031

[10] Ji L, Wang J, Teng X, Meyer TJ, Chen Z (2020) CoP Nanoframes as Bifunctional Electrocatalysts for Efficient Overall Water Splitting. ACS Catal 10 (1):412-419. https://doi:10.1021/acscatal.9b03623

[11] Wang H, Min S, Wang Q, Li D, Casillas G, Ma C, Li Y, Liu Z, Li L-J, Yuan J, Antonietti M, Wu T (2017) Nitrogen-Doped Nanoporous Carbon Membranes with Co/CoP Janus-Type Nanocrystals as Hydrogen Evolution Electrode in Both Acidic and Alkaline Environments. ACS Nano 11 (4):4358-4364. https://doi:10.1021/acsnano.7b01946

[12] Boppella R, Tan J, Yang W, Moon J (2019) Homologous CoP/NiCoP Heterostructure on N-Doped Carbon for Highly Efficient and pH-Universal Hydrogen Evolution Electrocatalysis. Adv Funct Mater 29 (6):1807976. https://doi:10.1002/adfm.201807976

[13] Xiao X, He C-T, Zhao S, Li J, Lin W, Yuan Z, Zhang Q, Wang S, Dai L, Yu D (2017) A general approach to cobalt-based homobimetallic phosphide ultrathin nanosheets for highly efficient oxygen evolution in alkaline media. Energy EnvironSci 10 (4):893-899. https://doi:10.1039/C6EE03145E

[14] Pu Z, Liu Q, Jiang P, Asiri AM, Obaid AY, Sun X (2014) CoP Nanosheet Arrays Supported on a Ti Plate: An Efficient Cathode for Electrochemical Hydrogen Evolution. Chem Mater 26 (15):4326-4329. https://doi:10.1021/cm501273s

[15] Wang P-c, Wan L, Lin Y-q, Wang B-g (2019) NiFe Hydroxide Supported on Hierarchically Porous Nickel Mesh as a High-Performance Bifunctional Electrocatalyst for Water Splitting at Large Current Density. ChemSusChem 12 (17):4038-4045. https://doi:10.1002/cssc.201901439

[16] Wang P, Lin Y, Wan L, Wang B (2020) Autologous growth of Fe-doped $Ni(OH)_2$ nanosheets with low overpotential for oxygen evolution reaction. Int J Hydrogen Energy 45 (11):6416-6424. https://doi.org/10.1016/j.ijhydene.2019.12.156

[17] Du H, Liu Q, Cheng N, Asiri AM, Sun X, Li CM (2014) Template-assisted synthesis of CoP nanotubes to efficiently catalyze hydrogen-evolving reaction. J Mater Chem A 2 (36):14812-14816. https://doi:10.1039/C4TA02368D

[18] Tian J, Liu Q, Cheng N, Asiri AM, Sun X (2014) Self-Supported $Cu_3P$ Nanowire Arrays as an

Integrated High-Performance Three-Dimensional Cathode for Generating Hydrogen from Water. Angew Chem Int Ed 53 (36):9577-9581. https://doi:10.1002/anie.201403842

[19] Guan C, Xiao W, Wu H, Liu X, Zang W, Zhang H, Ding J, Feng YP, Pennycook SJ, Wang J (2018) Hollow Mo-doped CoP nanoarrays for efficient overall water splitting. Nano Energy 48:73-80. https://doi.org/10.1016/j.nanoen.2018.03.034

[20] Niu Z, Qiu C, Jiang J, Ai L (2019) Hierarchical CoP–FeP Branched Heterostructures for Highly Efficient Electrocatalytic Water Splitting. ACS Sustainable Chem Engin 7 (2):2335-2342. https://doi:10.1021/acssuschemeng.8b05089

[21] Jin H, Wang J, Su D, Wei Z, Pang Z, Wang Y (2015) In situ Cobalt–Cobalt Oxide/N-Doped Carbon Hybrids As Superior Bifunctional Electrocatalysts for Hydrogen and Oxygen Evolution. J Am Chem Soc 137 (7):2688-2694. https://doi:10.1021/ja5127165

[22] Pan Y, Lin Y, Liu Y, Liu C (2016) A novel CoP/$MoS_2$-CNTs hybrid catalyst with Pt-like activity for hydrogen evolution. Catal Sci Technol 6 (6):1611-1615. https://doi:10.1039/C5CY02299A

[23] Wang P, Lin Y, Wan L, Wang B (2019) Construction of a Janus $MnO_2$.NiFe Electrode via Selective Electrodeposition Strategy as a High-Performance Bifunctional Electrocatalyst for Rechargeable Zinc–Air Batteries. ACS Appl Mater Interfaces 11 (41):37701-37707. https://doi:10.1021/acsami.9b12232

[24] Wang P, Wan L, Lin Y, Wang B (2019) Construction of mass-transfer channel in air electrode with bifunctional catalyst for rechargeable zinc-air battery. Electrochim Acta 320:134564. https://doi.org/10.1016/j.electacta.2019.134564

[25] Wang P, Jia T, Wang B (2020) A critical review: 1D/2D nanostructured self-supported electrodes for electrochemical water splitting. J Power Sources 474:228621. https://doi.org/10.1016/j.jpowsour.2020.228621

[26] Wang P, Jia T, Wang B (2020) Review—Recent Advance in Self-Supported Electrocatalysts for Rechargeable Zinc-Air Batteries. J Electrochem Soc 167 (11):110564. https://doi:10.1149/1945-7111/aba96e

[27] Wang P, Wang B (2020) Interface Engineering of Binder-Free Earth-Abundant Electrocatalysts for Efficient Advanced Energy Conversion. ChemSusChem n/a (n/a). https://doi:10.1002/cssc.202001293

[28] Li Z, Cui J, Liu Y, Li J, Liu K, Shao M (2018) Electrosynthesis of Well-Defined Metal–Organic Framework Films and the Carbon Nanotube Network Derived from Them toward Electrocatalytic

Applications. ACS Appl Mater Interfaces 10 (40):34494-34501. https://doi:10.1021/acsami.8b12854

[29] Yang X, Lu A-Y, Zhu Y, Hedhili MN, Min S, Huang K-W, Han Y, Li L-J (2015) CoP nanosheet assembly grown on carbon cloth: A highly efficient electrocatalyst for hydrogen generation. Nano Energy 15:634-641. https://doi.org/10.1016/j.nanoen.2015.05.026

[30] Che Q, Li Q, Chen X, Tan Y, Xu X (2020) Assembling amorphous (Fe-Ni)$Co_x$-OH/$Ni_3S_2$ nanohybrids with S-vacancy and interfacial effects as an ultra-highly efficient electrocatalyst: Inner investigation of mechanism for alkaline water-to-hydrogen/oxygen conversion. Appl Catal B 263:118338. https://doi.org/10.1016/j.apcatb.2019.118338

[31] Wang J-G, Hua W, Li M, Liu H, Shao M, Wei B (2018) Structurally Engineered Hyperbranched NiCoP Arrays with Superior Electrocatalytic Activities toward Highly Efficient Overall Water Splitting. ACS Appl Mater Interfaces 10 (48):41237-41245. https://doi:10.1021/acsami.8b11576

[32] Wang P, Lin Y, Wan L, Wang B (2020) Core–Shell Cu@CoP as Highly Efficient and Durable Bifunctional Electrodes for Electrochemical Water Splitting. Energy Fuels 34 (8):10276-10281. https://doi:10.1021/acs.energyfuels.0c01493

[33] Wang P, Xu Z, Lin Y, Wan L, Wang B (2020) Exceptional Performance of MOF-Derived N-Doped CoP and Fe-Doped CoOOH Ultrathin Nanosheets Electrocatalysts for Overall Water Splitting. ACS Sustainable Chem Engin 8 (24):8949-8957. https://doi:10.1021/acssuschemeng.0c01293

[34] Korányi TI (2003) Phosphorus promotion of Ni (Co)-containing Mo-free catalysts in thiophene hydrodesulfurization. Appl Catal A 239 (1):253-267. https://doi.org/10.1016/S0926-860X(02)00390-3

[35] Liu T, Li P, Yao N, Cheng G, Chen S, Luo W, Yin Y (2019) CoP-Doped MOF-Based Electrocatalyst for pH-Universal Hydrogen Evolution Reaction. Angew Chem 58 (14):4679-4684. https://doi:10.1002/anie.201901409

[36] Conway BE, Tilak BV (2002) Interfacial processes involving electrocatalytic evolution and oxidation of $H_2$, and the role of chemisorbed H. Electrochim Acta 47 (22):3571-3594. doi:https://doi.org/10.1016/S0013-4686(02)00329-8

[37] Liu C, Gong T, Zhang J, Zheng X, Mao J, Liu H, Li Y, Hao Q (2020) Engineering $Ni_2P$-$NiSe_2$ heterostructure interface for highly efficient alkaline hydrogen evolution. Appl Catal B 262:118245. https://doi.org/10.1016/j.apcatb.2019.118245

[38] Wang X-D, Xu Y-F, Rao H-S, Xu W-J, Chen H-Y, Zhang W-X, Kuang D-B, Su C-Y (2016) Novel

porous molybdenum tungsten phosphide hybrid nanosheets on carbon cloth for efficient hydrogen evolution. Energy Environl Sci 9 (4):1468-1475. https://doi:10.1039/C5EE03801D

[39] Liu Q, Tian J, Cui W, Jiang P, Cheng N, Asiri AM, Sun X (2014) Carbon Nanotubes Decorated with CoP Nanocrystals: A Highly Active Non-Noble-Metal Nanohybrid Electrocatalyst for Hydrogen Evolution. Angew Chem Int Ed 53 (26):6710-6714. https://doi:10.1002/anie.201404161

[40] Zhang R, Wang X, Yu S, Wen T, Zhu X, Yang F, Sun X, Wang X, Hu W (2017) Ternary $NiCo_2P_x$ Nanowires as pH-Universal Electrocatalysts for Highly Efficient Hydrogen Evolution Reaction. Adv Mater29 (9):1605502. https://doi:10.1002/adma.201605502

[41] Popczun EJ, McKone JR, Read CG, Biacchi AJ, Wiltrout AM, Lewis NS, Schaak RE (2013) Nanostructured Nickel Phosphide as an Electrocatalyst for the Hydrogen Evolution Reaction. J Am Chem Soc 135 (25):9267-9270. https://doi:10.1021/ja403440e

[42] Huang Z, Chen Z, Chen Z, Lv C, Meng H, Zhang C (2014) $Ni1_2P_5$ Nanoparticles as an Efficient Catalyst for Hydrogen Generation via Electrolysis and Photoelectrolysis. ACS Nano 8 (8):8121-8129. https://doi:10.1021/nn5022204

[43] Huang Z, Chen Z, Chen Z, Lv C, Humphrey MG, Zhang C (2014) Cobalt phosphide nanorods as an efficient electrocatalyst for the hydrogen evolution reaction. Nano Energy 9:373-382. https://doi.org/10.1016/j.nanoen.2014.08.013

[44] Liu B, Li H, Cao B, Jiang J, Gao R, Zhang J (2018) Few Layered N, P Dual-Doped Carbon-Encapsulated Ultrafine MoP Nanocrystal/MoP Cluster Hybrids on Carbon Cloth: An Ultrahigh Active and Durable 3D Self-Supported Integrated Electrode for Hydrogen Evolution Reaction in a Wide pH Range. AdvFunct Mater 28 (30):1801527. https://doi:10.1002/adfm.201801527

[45] Zhou H, Yu F, Huang Y, Sun J, Zhu Z, Nielsen RJ, He R, Bao J, Goddard Iii WA, Chen S, Ren Z (2016) Efficient hydrogen evolution by ternary molybdenum sulfoselenide particles on self-standing porous nickel diselenide foam. NatCommun 7 (1):12765. https://doi:10.1038/ncomms12765

[46] Mishra IK, Zhou H, Sun J, Qin F, Dahal K, Bao J, Chen S, Ren Z (2018) Hierarchical CoP/Ni5P4/CoP microsheet arrays as a robust pH-universal electrocatalyst for efficient hydrogen generation. Energy Environ Sci 11 (8):2246-2252. https://doi:10.1039/C8EE01270A

[47] Yu X, Wang M, Gong X, Guo Z, Wang Z, Jiao S (2018) Self-Supporting Porous CoP-Based Films with Phase-Separation Structure for Ultrastable Overall Water Electrolysis at Large Current Density. Adv

Energy Mater8 (34):1802445. https://doi:10.1002/aenm.201802445

[48] Chang B, Hao S, Ye Z, Yang Y (2018) A self-supported amorphous Ni–P alloy on a CuO nanowire array: an efficient 3D electrode catalyst for water splitting in alkaline media. Chem Commun 54 (19):2393-2396. https://doi:10.1039/C7CC09007B

[49] Jiang Y, Lu Y, Lin J, Wang X, Shen Z (2018) A Hierarchical MoP Nanoflake Array Supported on Ni Foam: A Bifunctional Electrocatalyst for Overall Water Splitting. Small Methods 2 (5):1700369. https://doi:10.1002/smtd.201700369

[50] Fu Q, Wu T, Fu G, Gao T, Han J, Yao T, Zhang Y, Zhong W, Wang X, Song B (2018) Skutterudite-Type Ternary Co1–xNixP3 Nanoneedle Array Electrocatalysts for Enhanced Hydrogen and Oxygen Evolution. ACS Energy Lett 3 (7):1744-1752. https://doi:10.1021/acsenergylett.8b00908

[51] Zhang H, Li X, Hähnel A, Naumann V, Lin C, Azimi S, Schweizer SL, Maijenburg AW, Wehrspohn RB (2018) Bifunctional Heterostructure Assembly of NiFe LDH Nanosheets on NiCoP Nanowires for Highly Efficient and Stable Overall Water Splitting. Adv Funct Mater 28 (14):1706847. https://doi:10.1002/adfm.201706847

[52] Tian J, Liu Q, Asiri AM, Sun X (2014) Self-Supported Nanoporous Cobalt Phosphide Nanowire Arrays: An Efficient 3D Hydrogen-Evolving Cathode over the Wide Range of pH 0–14. J Am Chem Soc 136 (21):7587-7590. https://doi:10.1021/ja503372r

[53] Menezes PW, Indra A, Das C, Walter C, Göbel C, Gutkin V, Schmeiβer D, Driess M (2017) Uncovering the Nature of Active Species of Nickel Phosphide Catalysts in High-Performance Electrochemical Overall Water Splitting. ACS Catal 7 (1):103-109. https://doi:10.1021/acscatal.6b02666

[54] Yuan C-Z, Zhong S-L, Jiang Y-F, Yang ZK, Zhao Z-W, Zhao S-J, Jiang N, Xu A-W (2017) Direct growth of cobalt-rich cobalt phosphide catalysts on cobalt foil: an efficient and self-supported bifunctional electrode for overall water splitting in alkaline media. J Mater Chem A 5 (21):10561-10566. https://doi:10.1039/C7TA01776F

[55] Feng Y, Yu X-Y, Paik U (2016) Nickel cobalt phosphides quasi-hollow nanocubes as an efficient electrocatalyst for hydrogen evolution in alkaline solution. Cheml Commun 52 (8):1633-1636. https://doi:10.1039/C5CC08991C